RAA 2019 Vol. **19** No. **4**, 52(8pp) doi: 10.1088/1674–4527/19/4/52
© 2019 National Astronomical Observatories, CAS and IOP Publishing Ltd.
http://www.raa-journal.org *http://iopscience.iop.org/raa*

***R**esearch in*
***A**stronomy and*
***A**strophysics*

Mineralogy of northern nearside mare basalts

Zhen-Chao Wang[1,2], Yun-Zhao Wu[2,3⋆], Xiao-Meng Zhang[4] and Yu Lu[5,6]

[1] Key Laboratory of Surficial Geochemistry, Ministry of Education, Department of Earth Sciences, Nanjing University, Nanjing 210023, China
[2] Key Laboratory of Planetary Sciences, Purple Mountain Observatory, Chinese Academy of Sciences, Nanjing 210034, China; *wu@pmo.ac.cn*
[3] CAS Center for Excellence in Comparative Planetology, Hefei 230026, China
[4] Xuzhou Bureau of Land and Resources, Xuzhou 221000, China
[5] School of Geographic and Oceanographic Sciences, Nanjing University, Nanjing 210023, China
[6] Jiangsu Center for Collaborative Innovation in Geographical Information Resource Development and Application, Nanjing 210023, China

Received 2018 May 26; accepted 2018 September 28

Abstract The mineralogy of mare basalts reflects the chemical composition of the magma source, as well as the physical and chemical environment of the rocks' formation. This is significant for understanding the thermal evolution of the Moon. In this study, the spatial distribution of mineralogy on the lunar northern nearside basalts was mapped using the Moon Mineralogy Mapper (M^3) data. The study area, which is an elongated mare, Mare Frigoris and northern Mare Imbrium, was mapped and characterized into 27 units based on multi-source data, including spectrum, terrain and element abundance. We extracted 177 M^3 spectra from fresh craters. Spectral parameters such as absorption center and band area ratio (BAR) were obtained through data processing. The variation of mafic minerals in this region was acquired by analyzing these parameters. The basaltic units in eastern Mare Frigoris, which are older, have been found to be dominated by clinopyroxene with lower CaO compared to the returned lunar samples; this is similar to older basaltic units in Mare Imbrium. The basaltic units of western Mare Frigoris and Sinus Roris which are younger have been found to be rich in olivine. The late-stage basalts in Oceanus Procellarum and Mare Imbrium show the same feature. These widespread olivine-rich basalts suggest uniqueness in the evolution of the Moon. Geographically speaking, Mare Frigoris is an individual mare, but the magma source region has connections with surrounding maria in consideration of mineral differences between western and eastern Frigoris, as well as mineral similarities with maria at the same location.

Key words: Moon — evolution — imaging spectroscopy — data analysis

1 INTRODUCTION

Mare basalt covers 17% of the surface of the Moon and accounts for approximately 1% of the lunar crust (Head 1976). Its spatial distribution, composition and volume record important information on the magmatic activity of the Moon. Research into its mineral components aids understanding of the magma source and characterizes the pressure, temperature, cooling rate and other physical parameters of the magmatic state and related processes. In addition, the mineralogy of mare basalts is an important scientific focus of lunar exploration.

Among lunar maria, Mare Frigoris is very special. Most maria are circular, however, Mare Frigoris is very long and narrow (approximately 1800 km long with a maximum width of 200 km). Although Mare Frigoris is a separate mare geographically, its basalts may be associated with the adjacent maria (such as western Mare Frigoris and Oceanus Procellarum, southern Mare Frigoris and northern

⋆ Corresponding author.

Mare Imbrium). Therefore, this long and narrow mare was chosen as the major research area for this study to analyze the variation in mineral compositions in different locations. Furthermore, it can be used as a comparison with the mineral compositions of adjacent maria (northern Mare Imbrium basalts) to discuss its role in the thermal evolution of the Moon.

Figure 1 shows the focus area of this study. It is centered around Mare Frigoris, including Sinus Roris in western and northern Mare Imbrium. Mare Frigoris is located in Procellarum KREEP Terrane (PKT) on the nearside of the Moon (Jolliff et al. 2000), at 56.0°N central latitude and 1.4°E central longitude. Its west side is linked to Oceanus Procellarum by Sinus Roris. Whitford-Stark (1990) drew the geological map of Mare Frigoris based on ground observation and data from the *Lunar Orbiter* program, and revealed that the oldest and youngest basalts were located in the northeast and southwest, respectively. Hiesinger et al. (2010) classified 37 geological units using the false color images of *Clementine* ultraviolet/visible (UV/VIS) data, and calculated the model age using the crater size-frequency distribution (CSFD) method. The results showed that the youngest basalts were located in Sinus Roris; four young Eratosthenian basalts were located in the middle of Mare Frigoris, to the North of crater Plato and northwest of crater Baily; the remaining old geological units were formed in the late Mare Imbrium, aged between 3.4 and 3.8 Ga. Kramer et al. (2015) divided Mare Frigoris into 26 geological units based on *Clementine*, *Lunar Prospector* (LP) and *Lunar Reconnaissance Orbiter* (*LRO*) data. With the exception of two units in the west, where the iron and titanium contents reached the levels of medium iron and low titanium, and medium iron and medium titanium, respectively, the majority of the remaining areas was characterized as high-alumina basalts, characterized by low titanium to extremely low titanium, low iron and high alumina.

The *Clementine* UV/VIS data range from 415 to 1000 nm with only five bands. The spectral resolution is low, which restricts reliable identification of the minerals. India's *Chandrayaan-1* Moon Mineralogy Mapper (M^3) data have a wider range of wavelengths and higher spectral resolution. They can approximate a continuous spectral curve, so as to more accurately infer the mineral composition. The study obtains the spectral absorption characteristics of fresh craters by using the M^3 data to identify the mineral composition of Mare Frigoris and northern Mare Imbrium. Then, it compares the composition with those of adjacent maria to discuss its regional geological significance.

2 DATA

The M^3 Level 2 (L2) data with spatial resolution of 140 m pixel^{-1} were used for the mineral analysis. In addition, this study adopts a variety of other data for the division of stratigraphic units. Of these, the standard *Clementine* color ratio composite (R, 750/415, G, 750/950, B, 415/750) map and the standard M^3 integrated band depth (IBD) composite (R: 1000 nm IBD; G: the 2000 nm IBD; and B: reflectance at 1480 nm) were used as base maps for separating basaltic units. In the two mosaic images the stitching traces between orbital boundaries are very obvious, which makes it difficult to separate different geologic units. The Lunar Reconnaissance Orbiter Camera (LROC) Wide Angle Camera (WAC) 7-channel composite (Wagner et al. 2015) and the *Chang'E-1* interference imaging spectroscopy (IIM) data calibrated in Wu et al. (2013) eliminate the tile-shaped splicing boundary. These non-trace mosaics are conducive to preparing the geological map, though they are partially missing and unable to completely cover the study area. Moreover, the M^3 images containing thermal emission radiation, the WAC low-Sun mosaic and 30 m LOLA DEM show morphology information and hence contribute to the separation of basaltic units (Wu et al. 2018a). The FeO and TiO_2 maps were from the original IIM 2C level data (Wu 2012). All the data except those from IIM were from the Planetary Data System (PDS).

3 METHODOLOGY

3.1 Separation of Stratigraphy

Stratigraphic division, which is important for the interpretation of mineralogy and geology, is not easy work because of space weathering, contamination by ejecta and lack of perfectly calibrated data. Following the methodology developed in Wu et al. (2018a), the separation of geologic units in this study was derived using diverse datasets including *Clementine* band ratio composite, FeO abundances, IIM color composite, LROC WAC mosaic composite, M^3 IBD, M^3 enhanced color and LROC WAC low-Sun image. All of these images were input in ArcGis and stretched for contrast enhancement.

3.2 Collection of Spectra

To avoid space weathering, the spectra from small fresh craters with diameters of $<\sim$1 km or slightly larger, and the mean spectra calculated from several pixels of the individual crater, have often been used in previous publica-

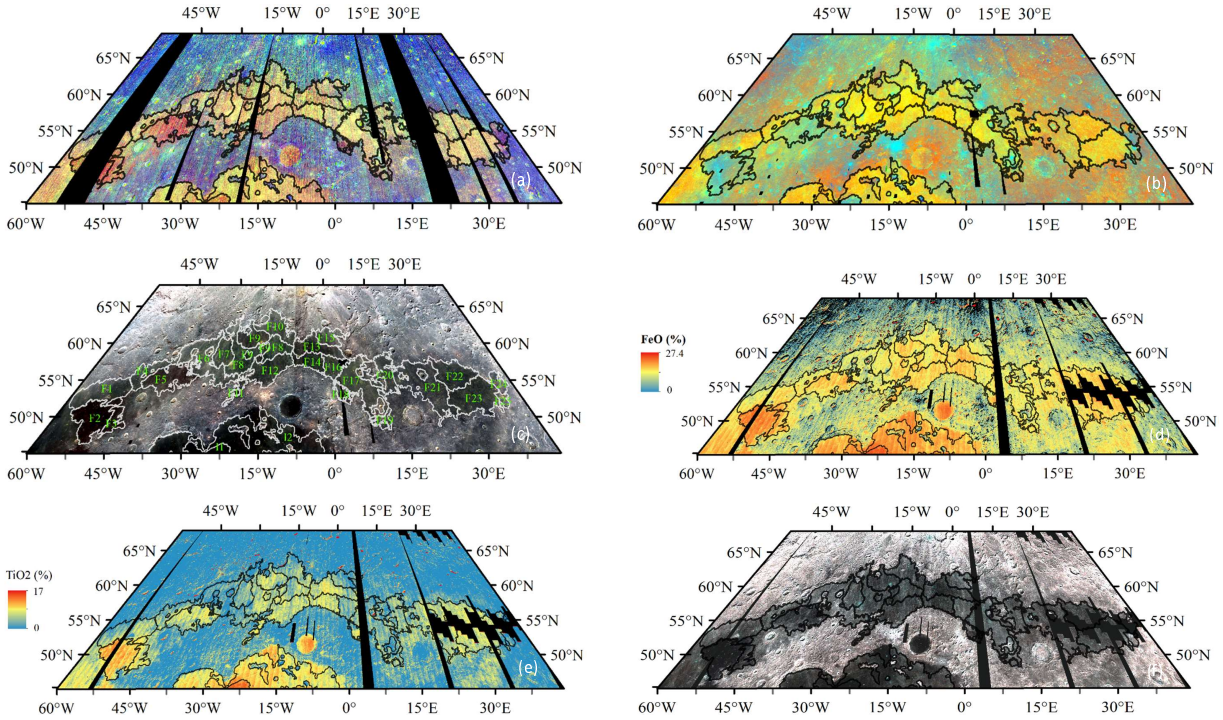

Fig. 1 Images of the study area, where *black*/*white* lines delineate the geological units classified in this study. (a) M^3 IBD image (R-1000 nm IBD; G-2000 nm IBD; B-albedo of 1548 nm). (b) *Clementine* color composite ratio image (R-750/415 nm, G-750/950 nm, B-415/750 nm). (c) *Clementine* false color composite image (R-950 nm; G-750 nm; B-415 nm), in which F1-F25 represent 25 geological units of Mare Frigoris, and I1 and I2 represent two geological units of Mare Imbrium. (d) The *Chang'E-1* IIM FeO content diagram. (e) IIM TiO_2 content diagram; (f) IIM false color composite image (R-891 nm; G-739 nm; B 618 nm).

tions (Kramer et al. 2008; Staid & Pieters 2001; Whitten et al. 2011; Kaur et al. 2013). The extracted spectra from craters with diameters of ∼1 km easily contain the compositions of underlying stratigraphy because craters of this size could excavate depths of approximately 84 m (Melosh 1989). If a crater has a lower resolution than that of M^3, the spectra are not from the fresh crater itself; instead, they contain shadows, melts and soils. Through trial-and-error in Wu et al. (2018a), a fresh crater with a diameter of 3 – 5 M^3 pixels is optimal to not only distinguish walls from shadows, but also to represent the top unit. Following Wu et al. (2018a), in this study we used fresh craters with diameters of 400 – 500 m to sample spectra, and they were from one high-quality pixel to reduce pixel mixing. In order to ensure that the craters are fresh, very high spatial-resolution LROC Narrow Angle Camera (NAC) data were used.

3.3 Spectral Parameter Acquisition

The mafic minerals (e.g., pyroxene and olivine) of mare basalts can be identified through their characteristic spectral absorption features. Pyroxene displays two absorption peaks, one at approximately 1000 nm (Band I) and another at approximately 2000 nm (Band II) (Adams 1974, 1975; Burns 1993; Cloutis 1985; Klima et al. 2007). In contrast, the olivine reflectance spectrum is revealed by a broad and asymmetric 1000 nm absorption, but lacks 2000 nm absorption (Adams 1975; Singer 1981; Burns 1993; Isaacson et al. 2014). The broad Band I absorption in olivine is caused by three distinct absorption bands (Burns 1993). The central absorption, located just beyond 1000 nm, is caused by iron in the M2 crystallographic site. The two weaker absorptions near 850 and 1250 nm are the result of iron in the M1 site (Burns 1993; Sunshine & Pieters 1998). The Band I "secondary" absorption near 1250 nm allows olivine to be detected when admixed with the spectrally "stronger" pyroxene.

The absorption band center is crucial for mineral identification. The Band I and Band II centers provide a qualitative way to access the composition of pyroxenes (Klima et al. 2007). The band centers are influenced by the amount of Fe^{2+} and Ca^{2+}. For example, with increasing Fe^{2+} and Ca^{2+}, the band centers move slightly to longer wavelengths (Burns 1993; Hazen et al. 1978). However, in the case of olivine-pyroxene mixtures, Band I is dependent

on the relative abundances of both olivine and pyroxene, which makes the interpretations problematic. The band area ratio (BAR), defined as the ratio between Band II and Band I absorption features, is useful for estimating the relative abundances of pyroxene and olivine in basalts (Cloutis et al. 1986; Gaffey et al. 1993). The BAR is inversely proportional to the olivine content, but increases linearly with pyroxene abundance (Gaffey et al. 1993; Cloutis et al. 1986).

Prior to calculating the absorption parameters, a B-spline function fitting is used to smoothen the spectral data to reduce the effects of spectral noise. The spectral curve after smoothing maintains a similar form and value as the original, with noise removed. To derive an accurate absorption band center, the spectral continuum should be removed. The continuum removal was performed using the convex hull method with 2497 nm as the right endpoint suggested in Wu et al. (2018a) to handle the reflectance increases in the longer wavelength. The band area refers to the cumulative value in absorption depths of the continuum function within the 1000 and 2000 nm band absorption characteristic peaks. They are represented by Band I Area and Band II Area, respectively.

4 RESULTS AND DISCUSSION

4.1 Stratigraphy

According to the unit division method mentioned above, this study area has been divided into 27 units, 25 units in Mare Frigoris and Sinus Roris and two units in northern Mare Imbrium. Kramer et al. (2015) excludes F24 from Mare Frigoris, however, in the LROC WAC and M^3 OP1B images, it is smooth and dark on the surface, and thus it is included in the scope of research. Owing to the serious loss of M^3 data around Lacus Mortis, it is impossible to extract the spectrum. Thus, it is not included in this study. Figure 1 shows the unit division results in the M^3 IBD image, *Clementine* color ratio composite image, IIM FeO and TiO_2 content diagram, and IIM false color composite image.

Figure 1(a) shows the M^3 (IBD) composite. In this figure, the highlands appear blue, whereas mare basalts appear yellow/green to orange according to the relative strength of mafic minerals. The darker the red hues of a unit are, the higher the olivine/pyroxene ratios (Staid et al. 2011). In Figure 1(a), the F1, F4 and F6 units are in yellow, and F2, F3 and F5 are in orange. F7, F8, F9 and F10 are in yellow-green. F11 and F12 are in orange-red. F13 and F15 are in orange-yellow, and F14, F16, F17 and F19 are in yellow-green. Three edge units, namely F18 in the south of crater Plato and F24 and F25 in the east of crater Plato, are in purple in the *Clementine* ratio color composite image (Fig. 1b), F18 is in red-purple and F24 is in blue-purple. A blue area in the *Clementine* ratio false color composite image indicates the high content of titanium in a unit.

4.2 Spectral Analysis

Figure 2 shows the average reflectance of fresh craters, as well as their average reflectance curves after continuum removal. They are divided into three groups according to the shape of the spectral curves (width and depth of absorption characteristic and spectral slope): G1 (F2, F3, F4 and F5 in western Mare Frigoris; F11 in central Mare Frigoris; and I1 in central northern Mare Imbrium), G2 (F18 in southern Mare Frigoris and F24 on the extreme eastern side of Mare Frigoris), and G3 (remaining units except those in G1 and G2). The spectra of most units have strong absorption characteristics at 1000 and 2000 nm. The absorption characteristics of five units in G1 at 1000 and 2000 nm are in the middle level of the three groups. They have absorption at 1300 nm and weak absorption at 2000 nm. The absorption characteristics of two units in Group 2 are special; they have the weakest absorption at 1000 and 2000 nm and a big slope. This may be because it is difficult to select a fresh crater in this region, hence it contains a mixture of soils, or because the region has a less crystallized composition. F24 is the oldest unit in Mare Frigoris, aged 3.77 Ga (Hiesinger et al. 2010). It has characteristics of low iron and titanium contents and a weak absorption in the spectral curve. The spectral curves of the units in G3 are highly consistent; they have the strongest absorption at 1000 and 2000 nm and weak absorption at 1300 nm.

Figure 3 shows the average 1000 nm and 2000 nm absorption center scatter plots of all units. As a comparison, the figure also shows the laboratory spectral data of natural pyroxene and synthetic pyroxene (Adams 1974; Klima et al. 2011). The wavelengths of the 1000 and 2000 nm absorption centers of synthetic low-Ca pyroxene, which better addresses the fundamental constraints of crystal structure and Ca-Mg-Fe content on reflectance spectra, are 900 to 930 nm and 1800 nm to 2100 nm, respectively. Those of synthetic high-Ca pyroxene are 950 nm to 1070 nm and 2260 nm to 2400 nm, respectively. G1 has the maximum absorption center wavelength, namely 985 nm to 1035 nm and 2181 nm to 2226 nm, respectively. The spectral curve has a wide and asymmetrical absorption peak at 1000 nm. The absorption peak is weak at 2000 nm, which is the olivine-dominated mineralogy. The absorption center wavelengths of G2 are 972 nm to 982 nm and

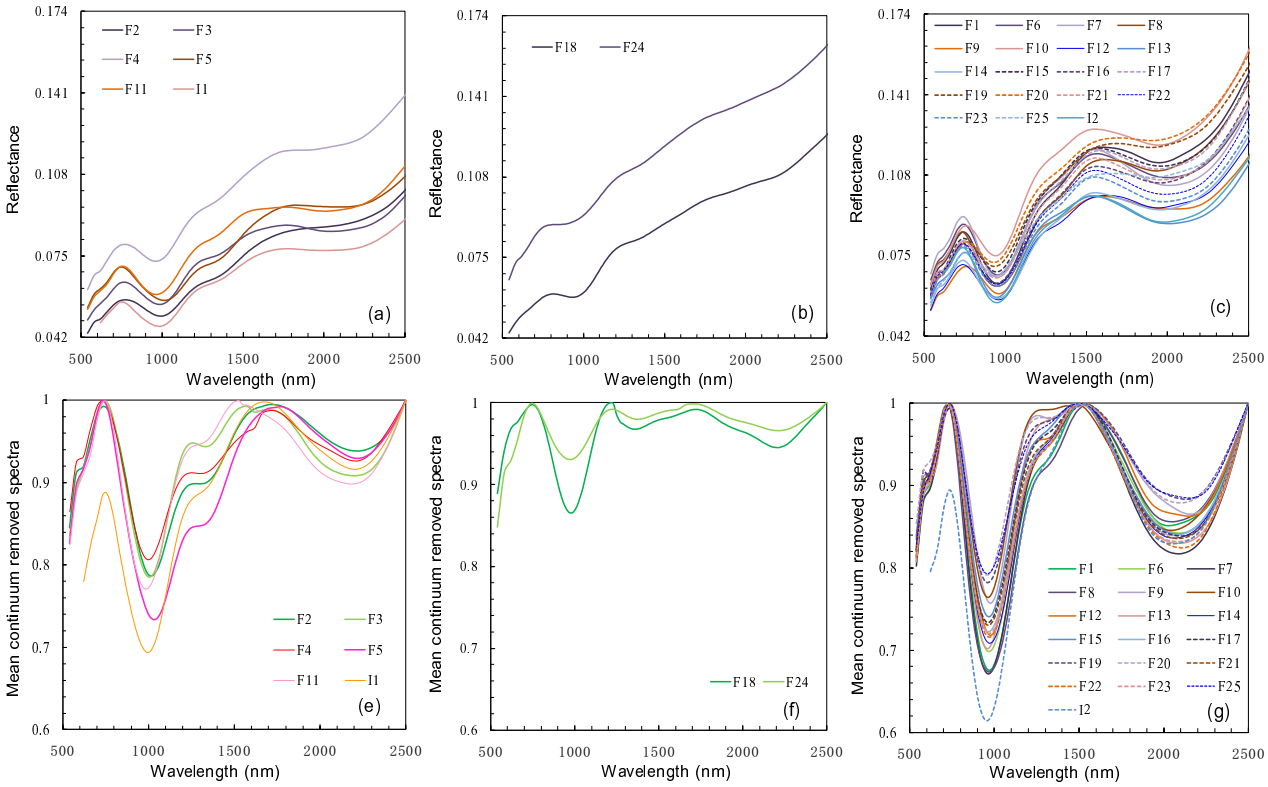

Fig. 2 The average reflectance curves of the different group units and their continuum-removed spectra. (a) G1: Strong absorption at 1000 nm and weak absorption at 2000 nm; (b) G2: Weak absorption at both 1000 and 2000 nm; (c) G3: Strong absorption at both 1000 and 2000 nm. The continuum-removed spectra for (a), (b) and (c) are (e), (f) and (g) respectively.

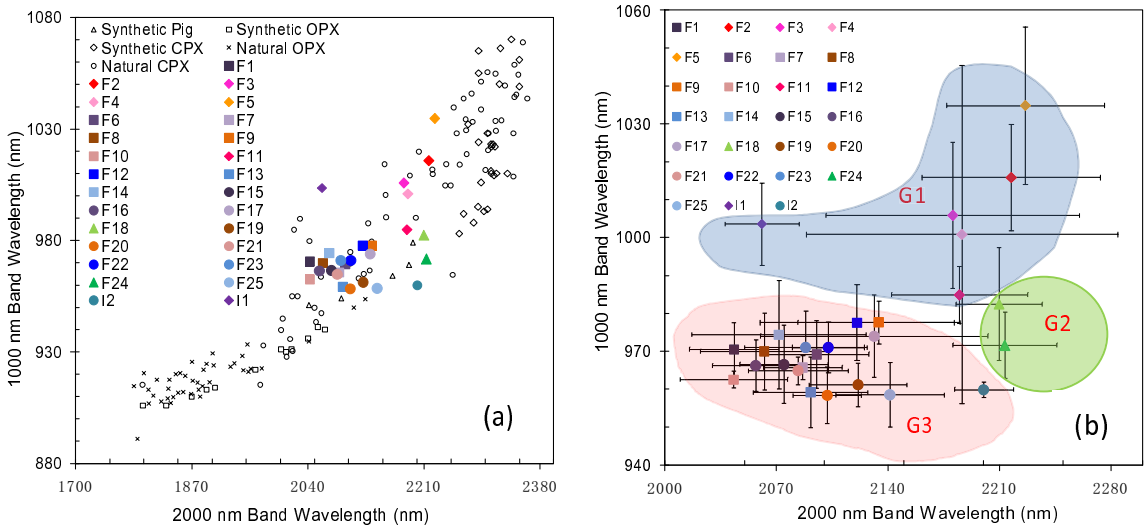

Fig. 3 Plot of the 1000 nm (Band I) versus 2000 nm (Band II) absorption centers. (a) Mean band center of each unit. The band centers of natural pyroxenes (Adams 1974; Cloutis & Gaffey 1991) and synthetic pyroxene (Klima et al. 2011) are also included. (b) Mean band center with error bars for each measurement. The error bars represent the standard deviation of each measurement. The *blue*, *green* and *pink* areas indicate groups G1, G2 and G3 respectively.

2210 nm to 2214 nm, respectively. Those of G3 are 958 nm to 978 nm and 2043 nm to 2141 nm, respectively, indicating rich monoclinic pyroxene; however, the content of pyroxene calcium is lower than that in the lunar samples.

Figure 3 shows the scatter plot of the absorption center wavelengths and BARs of the units of Mare Frigoris and northern Mare Imbrium. The BAR value is low in G1, ranging from 0.26 to 0.73, which is the olivine-dominated mineralogy. The BAR value is between 0.76 and 1.52 in

G3, which is the clinopyroxenes and olivine mixed mineral. The BARs of F18 and F24 in G2 are 0.85 and 0.83, respectively.

Figure 4 presents a distribution diagram of the 1000 nm absorption centers and BAR values of Mare Frigoris and northern Mare Imbrium. Overall, they both show a certain negative correlation, which is in line with the proportional change in olivine/pyroxene. This indicates that the minerals reflect the change from olivine domination to pyroxene domination. The olivine-dominated mineralogy in western Mare Frigoris and central Mare Imbrium has a long 1000 nm absorption center wavelength and a low BAR value. The clinopyroxene-dominated mineralogy in eastern central Mare Frigoris has the shortest 1000 nm wavelength and a high BAR value.

The change in the relative trends of mafic minerals in space in Mare Frigoris and northern Mare Imbrium can be seen intuitively from Figure 5. Western Mare Frigoris, Sinus Roris and central Mare Imbrium (F2, F3, F4, F5 and I1) have the longest 1000 nm absorption center wavelengths and the smallest BAR, dominated by olivine. Young basalts in Oceanus Procellarum are also dominated by olivine (Staid et al. 2011; Zhang et al. 2016). Further combining with the age data, the basalts in western Mare Frigoris, Sinus Roris, Oceanus Procellarum and Mare Imbrium are all found to be young basalts (F2, F3, F4 and F5 aged 1.3–1.7 Ga (Hiesinger et al. 2010), and I1 aged 2.35 Ga (Wu et al. 2018a)). Their similar olivine domination and age suggest that the late-stage thermal evolution of the Moon exhibits regularity over a larger scope.

The Mare Frigoris mineralogy in the north of crater Plato shows different absorption characteristics from those on its east and west sides. The 1000 nm absorption center on the west side is long with a small BAR value, whereas that on the east side is short with a large BAR value. The ratio of olivine to pyroxene on the west side is higher than that on the east. The 1000 nm absorption center wavelength and BAR value of mineralogy around the east of crater Aristoteles are 958.3 nm to 962.5 nm and 1.02 to 1.14, respectively. The ratio of olivine to pyroxene is low. The mineralogy in this area is old, aged over 3.56 Ga (Hiesinger et al. 2010). The basalts around the two craters are rich in low-Ca and medium-Ca pyroxene, which is consistent with the Mare Imbrium basalts in the north of the Mare Imbrium basin (Wu et al. 2018a). This may indicate that the deep source of east central Mare Frigoris basalt has a certain correlation with those of the northern Mare Imbrium basalts. These phenomena indicate that the deep source of Mare Frigoris may be consistent with surrounding adjacent lunar maria, despite being a geographical mare.

5 SUMMARY AND CONCLUSIONS

By comprehensive utilization of multi-source data and according to various characteristics of albedo, hue and topography, this study classified the units of maria on the northern nearside of the Moon in detail, analyzed the spectral absorption characteristics of different units, mapped the distribution of 1000 nm absorption center wavelengths and BAR values, and studied the mineral variation in different units.

The basalts in western Mare Frigoris and Sinus Roris have the highest ratio of olivine to pyroxene, i.e., they are rich in olivine. Similarly, the Eratosthenian basalts in northern Mare Imbrium (and Oceanus Procellarum) are also dominated by olivine (Staid et al. 2011; Varatharajan et al. 2014; Zhang et al. 2016). The basalts in central and eastern Mare Frigoris have low ratios of olivine to pyroxene. The mineralogy with the lowest ratio is located around crater Fontenelle on southern Mare Frigoris, and is rich in low-Ca to medium-Ca pyroxene. The old basalts in northern Mare Imbrium have similar composition. All of these phenomena indicate that, although Mare Frigoris is a geographical mare, the basalts of Mare Frigoris have different magma sources and have a certain correlation to the sources of adjacent maria.

The unsampled late-stage basalts are spectrally unique and hence they are compositionally unique and distinguished from older basalts. Some hypotheses have been suggested for the formation of these spectrally unique basalts. One explanation is that the olivine-rich Eratosthenian basalts were formed via partial melting from the ilmenite-rich mantle source and mixed with the residual KREEP layer beneath the anorthosite crust as it ascended to the surface (Zhang et al. 2015). Alternatively, Zhang et al. (2015) also suggests that the basalts were derived via partial melting of the mantle source that mixed with sinking ilmenite-rich KREEPy rocks. The young basalts in Mare Frigoris and Sinus Roris are rich in olivine, and the iron and titanium contents are also very high. The composition is similar to that of a large area of young basalts in Oceanus Procellarum and Mare Imbrium, which indicates that late-stage volcanism of the Moon occurred on a larger scale. The young basalts have the lowest amount of Mg among all the rocks on the Moon (e.g., Wu 2012; Crites & Lucey 2015). Data from the *Chang'E-3* rover's Active Particle-induced X-ray Spectrometer (APXS) show that the young basalts are characterized with high-FeO (22.24 wt.%), medium TiO_2 (4.31 wt.%) and high Al_2O_3 (12.11wt.%) (Wu et al. 2018b). The chemical and mineral data indicate that the

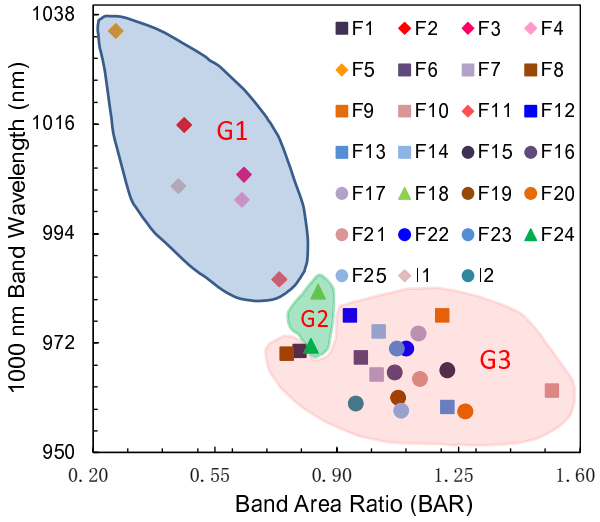

Fig. 4 BAR versus Band I center plot. The *blue*, *green* and *pink* areas indicate groups G1, G2 and G3, which correspond to the three groups from different units respectively.

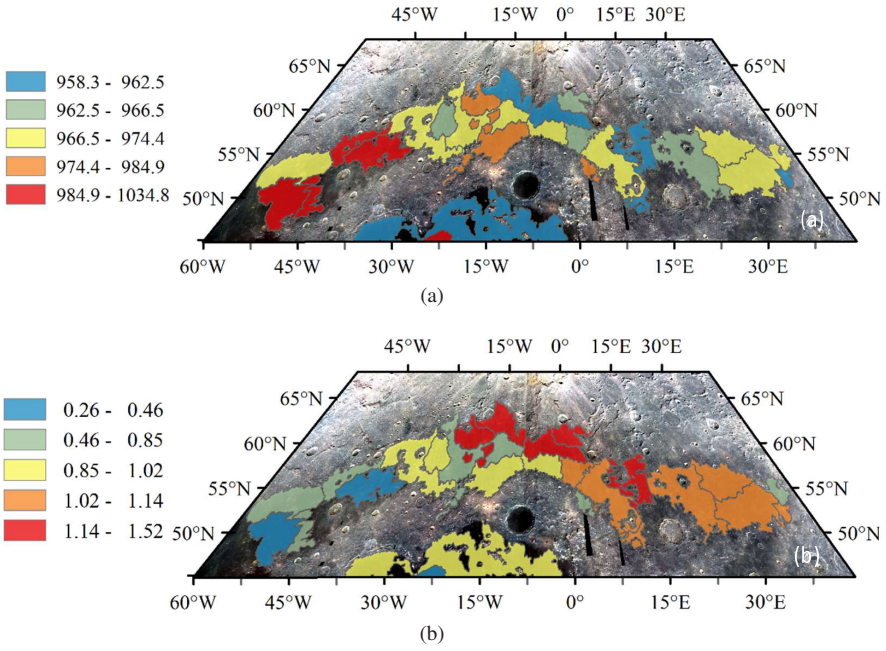

Fig. 5 Distribution of Band I center (a) and BAR (b) values. The base map is the *Clementine* false color composite image (R-950 nm; G-750 nm; B-415 nm).

young basalts do not have a KREEPy composition or affinity (Neal et al. 2015). Therefore, such a large-scale evolution and the unique composition show that their sources have experienced a dynamic evolution process rather than assimilation with KREEPy materials. In the future, samples of young basalts need to be collected for detailed petrological analysis. *Chang'E-5* will collect samples, and it is recommended that late-stage basalts be sampled.

Acknowledgements This research was supported by the Key Research Program of the Chinese Academy of Sciences (No. XDPB11), the National Natural Science Foundation of China (No. 11773087), the Macau Science and Technology Development Fund (103/2017/A and 0042/2018/A2), the Strategic Priority Research Program on Space Science, the Chinese Academy of Sciences (No. XDA15020302) and the Minor Planet Foundation of Purple Mountain Observatory. The M^3 Level 2 reflectance data were downloaded

from the website (*https://pds-geosciences.wustl.edu/*). The LROC WAC images were acquired from the LROC website (*http://wms.lroc.asu.edu/lroc*). The *Clementine* UV/VIS images were downloaded from the website (*http://pdsimage.wr.usgs.gov*).

References

Adams, J. B. 1974, J. Geophys. Res., 79, 4829

Adams, J. B. 1975, Interpretation of Visible and Near-infrared Diffuse Reflectance Spectra of Pyroxenes and Other Rockforming Minerals, Infrared & Raman Spectroscopy of Lunar & Terrestrial Minerals, 91

Burns, R. G. 1993, Mineralogical Applications of Crystal Field Theory (Cambridge: Cambridge Univ. Press), 575

Cloutis, E. A. 1985, Interpretive techniques for reflectance spectra of mafic silicates, M.S. Thesis, University of Hawai'i, Honolulu, Hawai'i

Cloutis, E. A., Gaffey, M. J., Jackowski, T. L., & Reed, K. L. 1986, J. Geophys. Res., 91, 11

Cloutis, E. A., & Gaffey, M. J. 1991, J. Geophys. Res., 96, 22

Crites, S. T., & Lucey, P. G. 2015, American Mineralogist, 100, 973

Gaffey, M. J., Bell, J. F., Brown, R. H., et al. 1993, Icarus, 106, 573

Hazen, R. M., Bell, P. M., & Mao, H. K. 1978, in Lunar and Planetary Science Conference Proceedings, 9, 2919

Head, III, J. W. 1976, Reviews of Geophysics and Space Physics, 14, 265

Hiesinger, H., Head, J. W., Wolf, U., Jaumann, R., & Neukum, G. 2010, Journal of Geophysical Research (Planets), 115, E03003

Isaacson, P. J., Klima, R. L., Sunshine, J. M., et al. 2014, American Mineralogist, 99, 467

Jolliff, B. L., Gillis, J. J., Haskin, L. A., Korotev, R. L., & Wieczorek, M. A. 2000, J. Geophys. Res., 105, 4197

Kaur, P., Bhattacharya, S., Chauhan, P., Ajai, & Kiran Kumar, A. S. 2013, Icarus, 222, 137

Klima, R. L., Pieters, C. M., & Dyar, M. D. 2007, Meteoritics and Planetary Science, 42, 235

Klima, R. L., Pieters, C. M., Boardman, J. W., et al. 2011, Journal of Geophysical Research (Planets), 116, E00G06

Kramer, G. Y., Jolliff, B. L., & Neal, C. R. 2008, Journal of Geophysical Research (Planets), 113, E01002

Kramer, G. Y., Jaiswal, B., Hawke, B. R., et al. 2015, Journal of Geophysical Research (Planets), 120, 1646

Melosh, H. J. 1989, Impact Cratering: A Geologic Process (New York, Oxford University Press (Oxford Monographs on Geology and Geophysics, No. 11))

Neal, C. R., Wu, Y. Z., Cui, X. Z., Peng, W. X., & Ping, J. S. 2015, in Lunar and Planetary Inst. Technical Report, 46, Lunar and Planetary Science Conference, 1641

Singer, R. B. 1981, J. Geophys. Res., 86, 7967

Staid, M. I., & Pieters, C. M. 2001, J. Geophys. Res., 106, 27887

Staid, M. I., Pieters, C. M., Besse, S., et al. 2011, Journal of Geophysical Research (Planets), 116, E00G10

Sunshine, J. M., & Pieters, C. M. 1998, J. Geophys. Res., 103, 13675

Varatharajan, I., Srivastava, N., & Murty, S. V. S. 2014, Icarus, 236, 56

Wagner, R. V., Speyerer, E. J., Robinson, M. S., et al. 2015, Lunar and Planetary Science Conference, 1473

Whitford-Stark, J. L. 1990, in Lunar and Planetary Science Conference Proceedings, 20, eds. V. L. Sharpton, & G. Ryder, 175

Whitten, J., Head, J. W., Staid, M., et al. 2011, Journal of Geophysical Research (Planets), 116, E00G09

Wu, Y. 2012, Geochim. Cosmochim. Acta, 93, 214

Wu, Y., Besse, S., Li, J.-Y., et al. 2013, Icarus, 222, 283

Wu, Y., Li, L., Luo, X., et al. 2018a, Icarus, 303, 67

Wu, Y., Wang, Z., Cai, W., & Lu, Y. 2018b, AJ, 155, 213

Zhang, J., Yang, W., Hu, S., et al. 2015, Proceedings of the National Academy of Science, 112, 5342

Zhang, X., Wu, Y., Ouyang, Z., et al. 2016, Journal of Geophysical Research (Planets), 121, 2063